Structural Engineering and Mechanics, *Vol. 62, No. 3 (2017) 273-279*
DOI: https://doi.org/10.12989/sem.2017.62.3.273

Meso-scale model for calculating the stiffness of filament wound composites considering fiber undulations

Chuangshi Shen*[1,2] and Xiaoping Han[1,2a]

[1]*School of Mechanics, Civil and Architecture, Northwestern Polytechnical University, Xi'an, 710072, China*
[2]*State Key Laboratory for Strength and Vibration of Mechanical Structures, Xi'an Jiaotong University, Xi'an,710049, China*

(Received May 2, 2016, Revised August 27, 2016, Accepted October 5, 2016)

Abstract. A meso-scale model is proposed to study filament-wound composites with fiber undulations and crossovers. First, the crossover and undulation region is classified as the circumferential undulation and the helical undulation. Next, the two undulations are separately regarded as a series of sub-models to describe the meso-structure of undulations by using meso-parameters such as fiber orientation, fiber inclination angle, resin rich area, fiber volume fraction and bundle cross section. With the meso-structure model and the classic laminate theory, a method for calculating the stiffness of filament wound composites is eventually established. The effects of the fiber inclination angle, the fiber and resin volume fraction and the resin rich area on the stiffness are studied. The numerical results show that the elastic moduli for the circumferential undulation region decrease to a great extent as compared with that of the helical undulation region. Moreover, significant decrease in the elastic and shear moduli and increase in the Poisson's ratio are also found for the resin rich area. In addition, thickness and bundle section have evident effect on the equivalent stiffness of the fiber crossover and the undulation region.

Keywords: filament wound composites; fiber crossover and undulation; meso-scale model; resin rich area; stiffness

1. Introduction

Filament wound composites are mostly used in oil-extraction, fluid transport, aerospace and aeronautic industries due to their specific strength ratio (Rousseau 1999, Moreno 2008, Morozov 2006). However, there are some inherent problems in the manufacturing method of filament-wound composite. For instance, during the winding process, the fiber tows in one direction interweave with the fiber bundles in the other direction. The interweave of the fiber tows, which produces the non-orthogonality of crossover geometries, increases the likelihood of defects such as the resin rich area (having higher resin volume fraction) and fiber crossover and undulation. Furthermore, cracks may originate from the fiber undulation region, and, as a consequence, lead to the premature leakage failure in fluid transport pipes and high pressure vessels. Therefore these regions with undulated fiber bundles will have tangible influence on the stiffness and damage evolution of the filament wound composite structures. These issues must be considered when trying to predict the actual behaviour of the structure.

Rousseau and Perreux (1999) studied the influence of winding patterns on the damage behavior of filament-wound pipes. Mechanical tests were carried out for the specimens subjected to progressive repeated loads so that the damage behavior under various loading was characterized. Increase of damage growths was observed with the interweaving degree of the tubes. Weeping tests under the closed-ended internal-pressure loading showed that the presence of fiber crossovers may cause the premature weeping of pipes. Another technique such as Acoustic emission (Ramirez 2015a) also be used to investigating the failure of the filament wound composite structure, the result indicates that damage first occurs in the vicinity of the fiber crossover region and then spread over the whole sample. In the same year, Ramirez (2014, 2015b) presented a continuum damage mechanics model to simulate the behavior and the burst of hyperbaric pressure vessel.

Mertiny (2004), Abdul (2011), Krishnan(2015), and Martins (2012, 2013, 2014) carried out the experiments under internal pressures and the axial forces to investigate the performance of multi-angle filament wound structures. In terms of failure stresses, observable modes of failure and the stress-strain curves, the results were compared with those of a baseline configuration made from a ± angle-ply lay-up. The influence of winding pattern on the mechanical response of filament wound glass/epoxy cylinders exposed to external pressure is also studied by testing cylindrical specimens having stacked layers with coincident patterns in a hyperbaric testing chamber (Moreno and Douchin 2008). Henry (2015) proposed an experimental method to back-calculate the undulation influenced ply properties from representative filament wound tubes using CLT together with other required ply properties determined via simpler conventional tests.

Based on the theory of Fourier series, Li (2008) presented a model for predicting the stiffness of filament-wound composite according to the micro-structure

*Corresponding author, Ph.D.
E-mail: chshshen@sina.com
[a]Professor
E-mail: xphan@nwpu.edu.cn

ISSN: 1225-4568 (Print), 1598-6217 (Online)

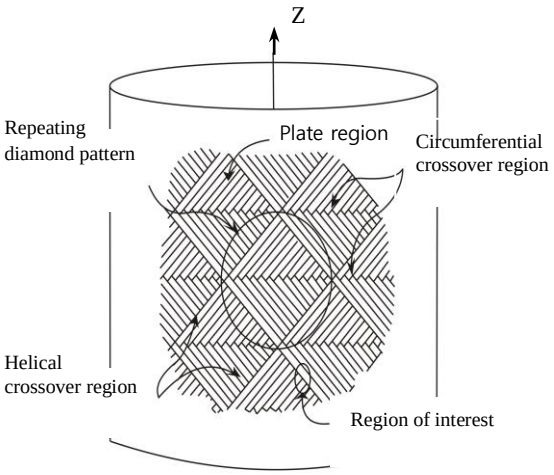

Fig. 1 The pattern of filament-wound structure

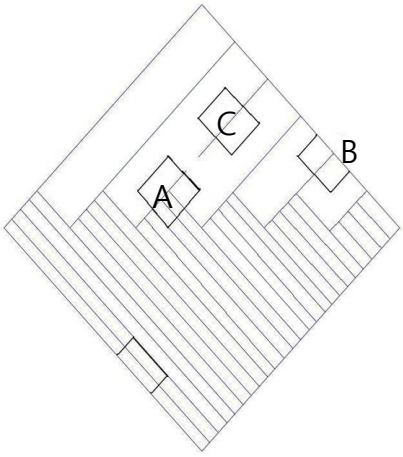

Fig. 2 The characteristic diamond-shaped unit

characteristic of filament-wound composite. In this model, the stiffness of the representative volume element (RVE) was treated as a field expanded by the 2D Fourier series.

On account of the meso-scale fiber undulation property, Sun *et al*. (2006) investigated the elastic modulus of filament wound composites. A representative filament winding pattern was divided into a laminate zone and a fiber undulation zone. Within the two zones, the elastic modulus was calculated respectively according to the classical laminate theory and the meso-scale fiber undulation situation. The whole elastic modulus for this pattern was eventually obtained through combining the two-zone elastic modulus with the area ratios of each zone.

In view of a modified classical lamination theory, a stiffness model for the crossover regions was developed by Pai and Jensen (1993, 2001).The local stiffness-coupling values predicted by this model were incorporated into a global finite-element model of filament-wound cylinder shell. 16 filament-wound cylinders with four different surface patterns were fabricated and then tested. The results showed that the finite element analysis improved the accuracy significantly when the stiffness coupling effects due to fiber undulations were accounted for in the analytical model.

Wen *et al*. (2012) conducted the experimental investigations on the strain characteristics of filament wound composite cylinder subjected to an axial tension. During loading, strains at three fiber crossing positions and one laminate region on the cylinder surface were measured by gauges. For all specimens, strains at fiber crossing positions were found larger than those of laminate region. This indicates that the fiber undulation caused by winding process has obvious affects on the mechanical response of filament wound composites.

In order to study the mechanical behavior of composites fabricated with the filament winding process, an experimental melti-instrumented study coupled with numerical analysis was proposed by Arellano *et al*. (2011). The strain values from the digital image correlation were validated as compared with gauge measurements and FEM simulations. Morozov (2006), Haris (2011) studied the influence of mosaic-shaped patterns on stress-strain field and conducted the design of thin-walled internally pressurized filament wound pressure vessel. The stress and strain distribution obtained by incorporating the effect of mosaic patterns are considerably different. The distribution of the stress and strain fields are not uniform along the length of the vessel and along its circumference.

Through the finite element analysis, Uddin *et al*. (2014) conducted the stress analysis of a filament wounding spinning composite disk with different filament winding mosaic patterns. The effects of filament winding mosaic pattern created during a filament winding process were investigated on the stress distributions and the strength of the filament wound spinning composite flywheel disk.

Zindel and Bakis (2011) developed a micro mechanics-based model to predict the axial modulus of elasticity of a filament-wound tube. The main innovation was the inclusion of nonlinear stress-strain behavior of the unidirectional composite material as well as the nonorthogonal undulation geometry inherent to the helical filament winding process. The impact of manufacturing parameters such as winding angle and number of rhombic-shaped patterns around the circumference of the tube was investigated.

The aim of the current work is to characterize the influence of fiber crossover and undulation on the mechanical performance of filament wound composite structures. By using the meso-parameters such as fiber orientation, fiber and resin volume fraction, fiber inclination angle and bundle cross section, a meso-scale model is proposed to analyze the meso-structure of filament wound composites with fiber undulations and crossovers. With this model and the classic laminate theory, a method for calculating the stiffness of fiber undulation and crossover region is therefore suggested.

2. Calculation model for the stiffness of fiber undulation and crossover region

2.1 Diamond-shaped patterns in filament-wound cylinders

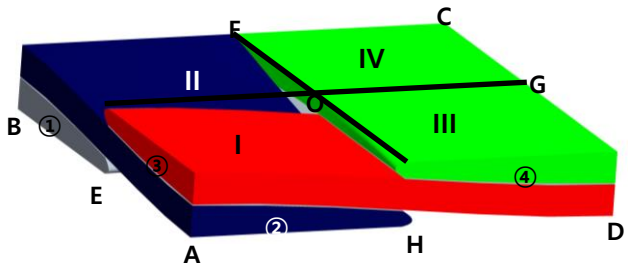

Fig. 3 The pattern for circumferential undulation region

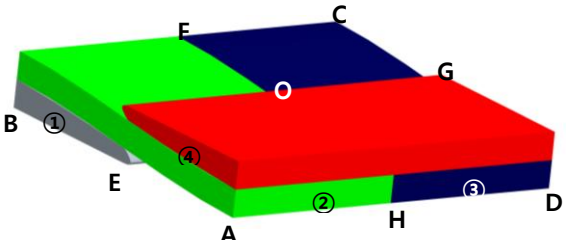

Fig. 4 The pattern for helical undulation region

A series of the repetitive diamond-shaped patterns are formed on the winding process of filament-wound composite, and it is plotted in Fig. 1. The repetitive unit is divided into three kind of regions as shown in Fig. 2. A-the circumferential undulation region, B-the helical undulation region and C-the uniformly laminated region. In the forming process of the circumferential undulation region, there are mutual cross and extrusion among the winding process. The pre-tension was applied to the fibers during the filament winding process, the shape of the cross section of the filaments changes, as shown in Fig. 3. The order of filament winding was filament yarn 1→2→3→4.The cross section of filament yarn 1 looks like a rectangle at the initial stage, as a result of the pre-tension of the filament yarn 2,the section at BE location is then transformed approximately to be a one-fourth ellipse. This is also the case for the sections of filament yarn 2 at AH location and the filament yarn 3 at AE location. Afterwards, as a result of the mutual extrusion among the winding filaments, the ellipse-like sections of filament yarn 3 at H location is transformed gradually to be a rectangle at D location. There exist similar variations of the section for the filament yarn 4.

The forming process for the helical undulation region is similar to that for the circumferential undulation region. The winding of filaments is also in a proper order as shown in Fig. 4, i.e., filaments yarn 1→2→3→4.

2.2 The meso-scale model for the undulation region

The circumferential undulation region and the helical undulation region are separately regarded as a series of sub-model on the basis of the reference surface paralleling to the filament-wound cylinder shell, as shown in Figs. 5 and 6.

The space structure model can be divided into M*N sub-models using M*N-2 parallel sections. Each sub-model has different fiber and resin volume fraction, winding angle and inclination angle of fiber tow against different location. The

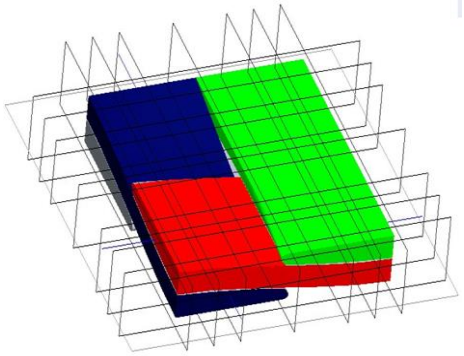

Fig. 5 Dispersing for meso-scale model region

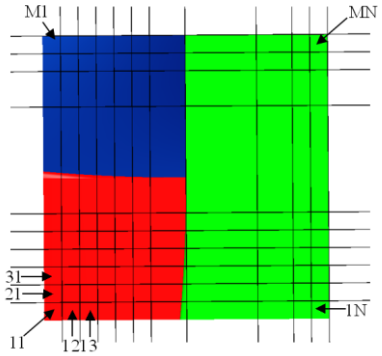

Fig. 6 Numbering sub-model

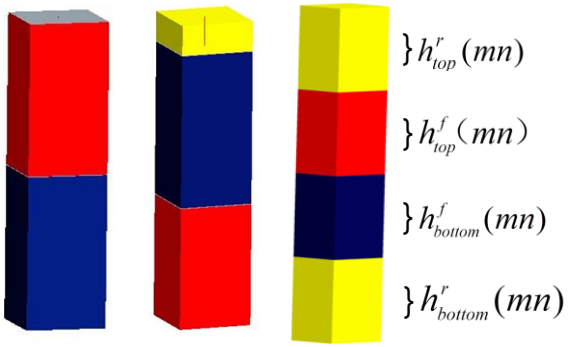

(a) 1-1 (b) 1-2 (c) m-n

Fig. 7 three representative sub-models

helical undulation region is a zonule of the resin rich area at the center of the region with the undulation region being symmetric and facing the center zonule while for the circumferential undulation the undulation region is unsymmetrical opposite to the center of the resin rich area. For the three representative sub-models shown in Fig. 7, the red and the blue represent the fiber tows, and the yellow represents the resin. Among them, 11 and 12 sub-model are at the edge of meso-scale model, and m-n sub-model is nearly at the center of meso-scale model.

2.3 Some parameters in each sub-model

The mid-surface of the undulation fiber tow is determined by a cosine function as

$$g(w)=\frac{a}{2}\cdot\cos(\frac{\pi\cdot w}{b}) \tag{1}$$

where $g(w)$ is the center line of undulating fiber to w, a is the thickness of fiber tow, w is the distance along the undulation and b is the length of undulation region.

In view of the different sections, the undulation region for the undulating fiber tow is divided into four districts, namely I, II, III and IV, as depicted in Fig. 3.

In district I, the fiber and resin volume fraction for each sub-model is calculated by

$$\begin{cases} h_{top}^{f}(mn)=a\cdot\cos(\dfrac{m-1}{M}\pi) \\ h_{bottom}^{f}(mn)=a\cdot\cos(\dfrac{n-1}{N}\pi) \\ h_{top}^{r}(mn)=a-a\cdot\cos(\dfrac{n-1}{N}\pi) \\ h_{bottom}^{r}(mn)=a-a\cdot\cos(\dfrac{m-1}{M}\pi) \end{cases} \tag{2}$$
$$m=1、2、.....M \qquad n=1、2、.....N$$

where $h_{top}^{f}(mn)$ and $h_{bottom}^{f}(mn)$ are the thicknesses of fiber tow respectively for the top and bottom layer in mn sub-model, $h_{top}^{r}(mm)$ and $h_{bottom}^{r}(mn)$ are the thicknesses of resin respectively for the top and bottom layer in mn sub-model, as shown in Fig. 7.

In district II and III, the fiber and resin volume fraction for each sub-model is determined by

$$\begin{cases} h_{top}^{f}(mn)=\dfrac{2(m-M/2)}{M}\left(a-a\cdot\cos(\dfrac{n-1}{N}\pi)\right)+a \\ h_{bottom}^{f}(mn)=a\cdot\cos(\dfrac{m-1}{M}\pi) \\ h_{top}^{r}(mn)=2a-h_{f}^{up}(mn)-h_{r}^{up}(mn) \\ h_{bottom}^{r}(mn)=0 \end{cases} \tag{3}$$
$$m=1、2、.....M \qquad n=1、2、.....N$$

In district IV, the fiber and resin volume fraction for each sub-model is determined by

$$\begin{cases} h_{top}^{f}(mn)=\dfrac{2(m-M/2)}{M}\left(a-a\cdot\cos(\dfrac{n-1}{N}\pi)\right)+a \\ h_{bottom}^{f}(mn)=\dfrac{2(n-N/2)}{N}\left(a-a\cdot\cos(\dfrac{m-1}{M}\pi)\right)+a \\ h_{top}^{r}(mn)=a-h_{f}^{up}(mn) \\ h_{bottom}^{r}(mn)=a-h_{r}^{up}(mn) \end{cases} \tag{4}$$
$$m=1、2、.....M \qquad n=1、2、.....N$$

Considering that the helical undulation region is symmetric about the center, the fiber and resin volume fraction for each sub-model is obtained as

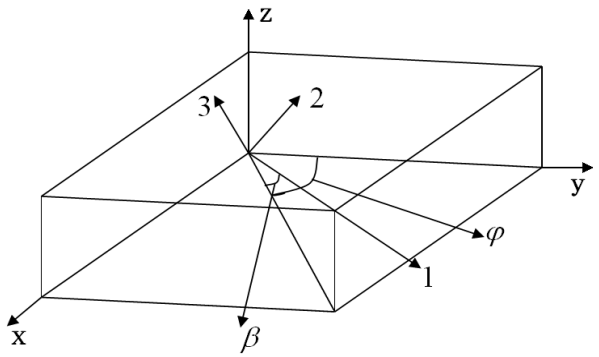

Fig. 8 The relation of the local coordinate system and the global coordinate system

$$\begin{cases} h_{top}^{f}(mn)=a\cdot\cos(\dfrac{m-1}{M}\pi) \\ h_{bottom}^{f}(mn)=a\cdot\cos(\dfrac{n-1}{M}\pi) \\ h_{top}^{r}(mn)=0 \\ h_{bottom}^{r}(mn)=a-a\cdot\cos(\dfrac{m-1}{M}\pi) \end{cases} \tag{5}$$
$$m=1、2、.....M \qquad n=1、2、.....N$$

In the meso-scale model, inclination angles of undulating fiber tow vary with the location, the following equation is chosen to calculate the inclination angles

$$\theta^{f}(mn)=\begin{cases} \arctan\left(-\dfrac{a\pi}{4L}\sin(\dfrac{\pi}{2M}\left(m-1/2\right))\right) \\ \arctan\left(-\dfrac{a\pi}{4L}\sin(\dfrac{\pi}{2N}\left(n-1/2\right))\right) \end{cases} \tag{6}$$

2.3 The effective stiffness of the undulation region

The curved fiber-bundles can be regarded as an assembly of a large number of infinitesimal segments in the undulation region. Hence, the laminated plate theory is applicable for each segment along the undulating direction. The equivalent stiffness of composites can be obtained through the two transformations in sequence as shown in Fig. 8, in which coordinate system $\bar{x}-\bar{y}-\bar{z}$ is the one revolving 90−φ from the global coordinate x-y-z while 1-2-3 is the local coordinate system. In the first transformation, the 3D stiffness parameters of undulating tow in the system 1-2-3 are transformed to be the one in the system $\bar{x}-\bar{y}-\bar{z}$ as

$$\left[\overline{C}^{f}(mn)\right]=[T_1]^{-1}\left[C^{f}(mn)\right][T_1]^{T} \tag{7}$$

with the transform matrix being

$$T_1=\begin{bmatrix} \cos(\beta)^2 & 0 & \sin(\beta)^2 & 0 & 2\sin(\beta)\cos(\beta) & 0 \\ 0 & 1 & 0 & 0 & 0 & 0 \\ \sin(\beta)^2 & 0 & \cos(\beta)^2 & 0 & -2\sin(\beta)\cos(\beta) & 0 \\ 0 & 0 & 0 & \cos(\beta) & 0 & -\sin(\beta) \\ -\sin(\beta)\cos(\beta) & 0 & \sin(\beta)\cos(\beta) & 0 & \cos(\beta)^2-\sin(\beta)^2 & 0 \\ 0 & 0 & 0 & \sin(\beta) & 0 & \cos(\beta) \end{bmatrix} \tag{8}$$

Table 1 Comparison of the results

	E_1/GPa	E_2/GPa	G_{12}/GPa	v_{12}
Majid (2011)	12.0	20.50	11.5	0.380
Meso-model	11.16	19.20	11.30	0.355

Then the 3D stiffness parameters of undulating tow in the system $\bar{x}-\bar{y}-\bar{z}$ are transformed to be the one in the system *x*-*y*-*z* as

$$\left[\overline{\overline{C}}^{f}(mn)\right]=\left[T_2\right]^{-1}\left[\overline{C}^{f}(mn)\right]\left[T_2\right]^{T} \tag{9}$$

with the transform matrix being

$$T_2=\begin{bmatrix} \cos(\varphi)^2 & \sin(\varphi)^2 & 0 & 0 & 0 & 2\sin(\varphi)\cos(\varphi) \\ \sin(\varphi)^2 & \cos(\varphi)^2 & 0 & 0 & 0 & -2\sin(\varphi)\cos(\varphi) \\ 0 & 0 & 1 & 0 & 0 & 0 \\ 0 & 0 & 0 & \cos(\varphi) & -\sin(\varphi) & 0 \\ 0 & 0 & 0 & \sin(\varphi) & \cos(\varphi) & 0 \\ -\sin(\varphi)\cos(\varphi) & \sin(\varphi)\cos(\varphi) & 0 & 0 & 0 & \cos(\varphi)^2-\sin(\varphi)^2 \end{bmatrix} \tag{10}$$

Thus the compliance parameters of undulating tow in the system *x*-*y*-*z* is obtained as

$$\left[\overline{\overline{S}}^{f}(mn)\right]=\left[\overline{\overline{C}}^{f}(mn)\right]^{-1} \tag{11}$$

With the elastic engineering constants of undulating tow in the sub-model mn, Eq. (11) can be expressed as

$$\begin{cases} E_1^f(mn)=\dfrac{1}{\overline{\overline{S}}^{f}_{f,11}(mn)} & E_2^f(mn)=\dfrac{1}{\overline{\overline{S}}^{f}_{22}(mn)} & E_3^f(mn)=\dfrac{1}{\overline{\overline{S}}^{f}_{33}(mn)} \\ G_{23}^f(mn)=\dfrac{1}{\overline{\overline{S}}^{f}_{f,44}(mn)} & G_{13}^f(mn)=\dfrac{1}{\overline{\overline{S}}^{f}_{f,55}(mn)} & G_{f,12}(mn)=\dfrac{1}{\overline{\overline{S}}^{f}_{66}(mn)} \\ v_{23}^f(mn)=\dfrac{\overline{\overline{S}}^{f}_{23}(mn)}{\overline{\overline{S}}^{f}_{33}(mn)} & v_{13}^f(mn)=\dfrac{\overline{\overline{S}}^{f}_{13}(mn)}{\overline{\overline{S}}^{f}_{33}(mn)} & v_{f,12}(mn)=\dfrac{\overline{\overline{S}}^{f}_{12}(mn)}{\overline{\overline{S}}^{f}_{11}(mn)} \end{cases} \tag{12}$$

By using the in-parallel and in-series mixture rule, the engineering elastic constants for the sub-model are obtained as

$$\begin{cases} E_1^{sub}(mn)=V^f(mn)E_1^f(mn)+V^r(mn)E^r(mn) \\ E_2^c(mn)=V^f(mn)E_2^f+V^r(mn)E^r(mn) \\ E_3^{sub}(mn)=E^r(mn)E_3^f(mn)\Big/\left(E^r(mn)V^f(mn)(mn)+E_3^fV^r(mn)\right) \\ G_{13}^{sub}(mn)=G^r(mn)G_{13}^f(mn)\Big/\left(G^r(mn)V^f(mn)+G_{13}^f(mn)V^r(mn)\right) \\ G_{23}^{sub}(mn)=G^r(mn)G_{23}^f(mn)\Big/\left(G^r(mn)V^f(mn)+G_{23}^f(mn)V^r(mn)\right) \\ G_{12}^{sub}(mn)=G^r(mn)V^r(mn)+G_{12}^f(mn)V^f(mn) \\ v_{12}^{sub}(mn)=V^f(mn)v_{12}^f(mn)+V^r(mn)v^r(mn) \\ v_{13}^{sub}(mn)=V^f(mn)v_{13}^f(mn)+V^r(mn)v^r(mn) \\ v_{23}^{sub}(mn)=V^f(mn)v_{23}^f(mn)+V^r(mn)v^r(mn) \end{cases} \tag{13}$$

Superscript sub represents sub-model, f represents fiber tow, *r* represents resin. Where V^f (mn) and V^r (mn) are the volume fractions respectively for fiber and resin in the sub-model, and calculated by

$$V^r(mn)=\frac{h^r(mn)}{a}\quad V^f(mn)=1-V^r(mn) \tag{14}$$

With the engineering elastic constants of undulating tow for each sub-model, the engineering elastic constants for the overall meso-structure model are eventually determined by averaging all the sub-models, i.e.

$$\begin{cases} E_i=\dfrac{1}{N^2}\displaystyle\sum_{m=1}^{N}\sum_{n=1}^{N}E_i^{sub}(mn) \\ G_{ij}=\dfrac{1}{N^2}\displaystyle\sum_{m=1}^{N}\sum_{n=1}^{N}G_{ij}^{sub}(mn) \qquad i,j=1,2,3 \\ v_{ij}=\dfrac{1}{N^2}\displaystyle\sum_{m=1}^{N}\sum_{n=1}^{N}v_{ij}^{sub}(mn) \end{cases} \tag{15}$$

3. Results and discussion

3.1 Results

In order to validate the meso-structure model, the material experimentally studied by Majid (2011) was re-examined.The layup of the cylinder is $[\pm 55]_4$, and the volume fraction of tow is 60%. The elastic constants are E_f=73GPa and v_f=0.22 for the fiber, and E_r=3.6GPa and v_r=0.4 for the resin. The results from the present calculation are listed in Table 1 as compared with the experiment ones (Majid 2011). It is seen that they are in a very good agreement.

3.2 Effect of the position in the undulating region on the elastic constants

The elastic constants of the undulation regions vary with the position in the undulation region, which are plotted as 3D contours in Figs. 9 and 10 including those for the circumferential undulation and the helical undulation region respectively. In the two figures, E_1 and E_2 are the effective moduli in the axial and hoop directions respectively, G_{12} is the effective in-plane shear modulus, and v_{12} is the effective in-plane Poisson's ratio. It is seen that these elastic constants apparently changes with positions in the undulation region.

It is seen from Fig. 9 that E_1, E_2 and G_{12} decrease significantly while v_{12} increases slightly at the center of the undulation. This is because the undulation center is a resin rich area with bigger inclination angles at the center for the circumferential undulation region, resulting in an apparent variation of the elastic constants.

It is seen from Fig. 10 that E_1, E_2 and G_{12} decrease significantly and v_{12} increase slightly along a zonule at the center of undulation. This is due to the reason that the zonule area is a resin rich area.

In Tables 2 and 3 are listed the elastic constants at the edge point A and the center point O (see Figs. 3 and 4) respectively in the circumferential undulation and in the helical undulation region. It is seen from Table 2 that,

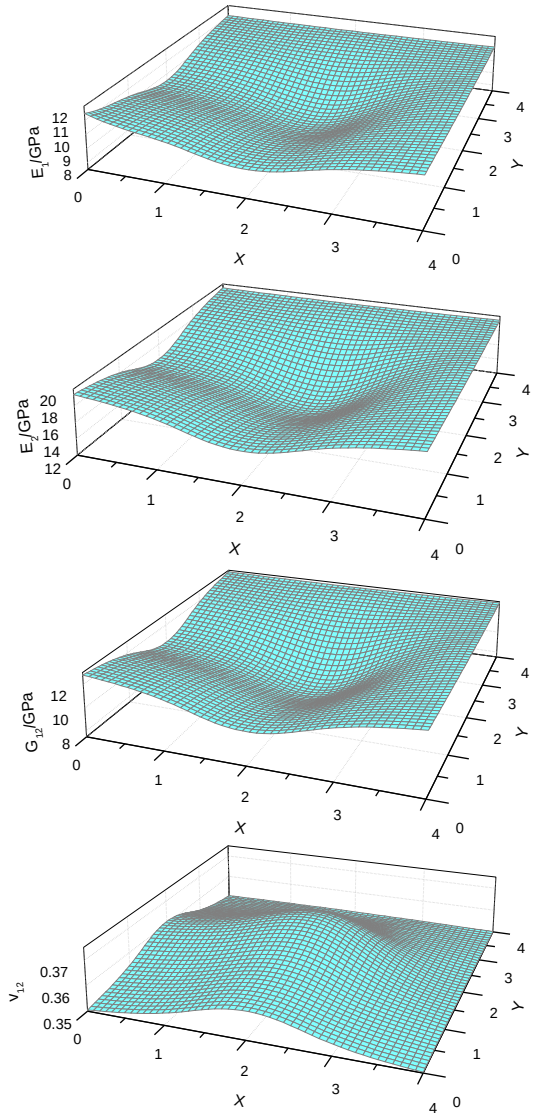

Fig. 9 The elastic constants for the circumferential undulation region

Table 2 Comparison of elastic constants in the circumferential undulation region

Position	E_1/GPa	E_2/GPa	E_3/GPa	G_{12}/GPa	v_{12}
Point A	11.5	19.35	12.8	12.8	0.350
Point O	8.11	13.10	9.20	8.25	0.370

compared with those at point O, E_1, E_2, E_3 and G_{12} at point A in the circumferential undulation decrease respectively by 29.5%, 32.3%, 28.1% and 45.5% while ν12 increases by 5.6%. It is seen from Table 3 that, compared those at point O, E_1, E_2, E_3 and G_{12} at point A in the helical undulation region decrease respectively by 13.5%, 16%, 14% and 14% while v_{12} increases by 2.8%. This shows that the elastic constants at point O (in a resin rich area) drop much more in the circumferential undulation region than in the helical undulation region.

3.3 Effect of the thickness of the filament bundle on the elastic constants

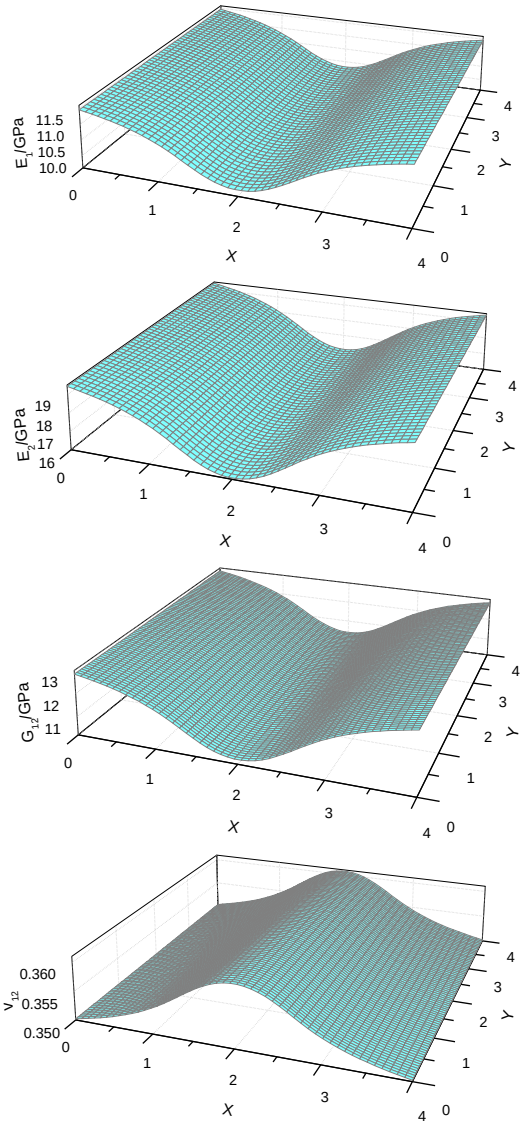

Fig. 9 The elastic constants for the helical undulation region

Table 3 Comparison of elastic constants in the helical undulation region

Position	E_1/GPa	E_2/GPa	E_3/GPa	G_{12}/GPa	v_{12}
Point A	11.46	19.42	12.85	12.84	0.3502
Point O	9.91	16.30	11.05	10.55	0.3600

The thickness of winding fiber bundles has great influence on the meso-scale model of filament crossover region.In order to avoid to repetition,the establishment of a quarter model study, the thickness of the filament yarn will be 0.3, 0.4 and 0.5 mm respectively, for instance, with ±55° winding angle.

In Table 4 are listed the elastic constants at point A and point O in the undulation region for different thickness of the filament yarn. It is seen that E_1, E_2 and G_{12} decrease with the thickness, while v_{12} increase slightly with the thickness. Along with the increase for the filament yarn thickness, E_1 at point A decreases by 8.3% and 13.8%; E_1 at the spot O drop by 10.2% and 15.9%; E_2 at the spot A drop by 10.1% and 16.3%; E_2 at the spot O drop by 12.3% and

Table 4 Comparison of elastic constants for different thickness of the filament yarn

	E_1/GPa		E_2/GPa		G_{12}/GPa		ν_{12}	
	Point A	Point O	Point A	Point O	Point A	Point O	Point A	Point O
0.3	11.5	9.91	19.4	16.3	12.8	10.6	0.350	0.3600
0.4	10.5	8.9	17.5	14.3	11.4	9.10	0.3565	0.3663
0.5	9.88	8.33	16.3	13.1	10.5	8.25	0.3602	0.3701

19.6%; G_{12} at the spot A drop by 11.3% and 18.1%; G_{12} at the spot O drop by 13.7% and 21.8%. Comparing the spot A with the spot O, the elastic constants at the spot O show more obvious effect for the thickness of the filament yarn, namely the elastic performance at the resin rich area in the undulation region show a evident drop with the increase of the thickness of the filament yarn.

4. Conclusions

In this paper, by using meso-parameters such as fiber orientation, fiber inclination angle, resin and fiber volume fraction, the thickness of the filament yarn, and bundle cross section, a meso-scale model was proposed to analyze the meso-structure of filament wound composites with fiber undulations and crossovers. From the current work, following conclusion can be made.

- The elastic constants remarkably vary with the position in the undulation region. The moduli at the resin rich area drop significantly.
- Compared with that in the circumferential undulation region, the variation of elastic constants in the helical undulation region is more apparent.
- With the increase for the filament yarn thickness, the elastic constants at the resin area in the undulation region show a evident drop

References

Arellano, M.T., Crouzeix, L., Douchin, B., Collombet, F., Moreno, H.H. and Velázquez, J.G. (2010), "Strain field measurement of filament-wound composites at ±55° using digital image correlation: an approach for unit cells employing flat specimens", *Compos. Struct.*, **92**(10), 2457-2464.

Henry, T.C., Bakis, C.E. and Smith, E.C. (2015), "Determination of effective ply-level properties of filament wound composite tubes loaded in compression", *Jo. Test. Eval.*, **43**(1), 96-107.

Hernández-Moreno, H., Douchin, B., Collombet, F., Choqueuse, D. and Davies, P. (2008), "Influence of winding pattern on the mechanical behavior of filament wound composite cylinders under external pressure", *Compos. Sci. Technol.*, **68**(3-4), 1015-1024.

Jensen, D.W. and Pai, S.P. (1993), "Influence of local fiber undulations on the global buckling behavior of filament-wound cylinders", *J. Reinf. Plast. Compos.*, **12**(8), 865-875.

Krishnan, P., Majid, M.S.A., Afendi, M., Gibson, A.G. and Marzuki, H.F.A. (2015), "Effects of winding angle on the behaviour of glass/epoxy pipes under multiaxial cyclic loading", *Mater. Des.*, **88**, 196-206.

Li, J., Wen, W. and Cui, H. (2008), "Predicting stiffness of filament-wound composite based on fourier series", *Fuhe Cailiao Xuebao/acta Materiae Compositae Sinica*, **25**(5), 169-174.

Majid, M.A., Assaleh, T.A., Gibson, A.G., Hale, J.M., Fahrer, A., Rookus, C.A.P. and Hekman, M. (2011), "Ultimate elastic wall stress (uews) test of glass fibre reinforced epoxy (gre) pipe", *Compos. Part A Appl. Sci. Manuf.*, **42**(10), 1500-1508.

Martins, L.A.L., Bastian, F. L., and Netto, T. A. (2014), "Reviewing some design issues for filament wound composite tubes", *Materials & Design*, **55**(6), 242-249.

Martins, L.A.L., Bastian, F.L. and Netto, T.A. (2012), "Structural and functional failure pressure of filament wound composite tubes", *Mater. Des.*, **36**, 779-787.

Martins, L.A.L., Bastian, F.L. and Netto, T.A. (2013), "The effect of stress ratio on the fracture morphology of filament wound composite tubes", *Mater. Des.*, **49**, 471-484.

Mertiny, P., Ellyin, F. and Hothan, A. (2004), "An experimental investigation on the effect of multi-angle filament winding on the strength of tubular composite structures", *Compos. Sci. Technol.*, **64**(1), 1-9.

Morozov, E.V. (2006), "The effect of filament-winding mosaic patterns on the strength of thin-walled composite shells", *Compos. Struct.*, **76**(1-2), 123-129.

Pai, S.P. and Jensen, D.W. (2001), "Influence of fiber undulations on buckling of thin filament-wound cylinders in axial compression", *J. Aerosp. Eng.*, **14**(1), 12-20.

Rahman, H. and Mian, H.H. (2011), "Influence of mosaic patterns on the structural integrity of filament wound composite pressure vessels", *Int. J. Struct. Integ.*, **66**(3), 185-188.

Ramirez, J.P.B., Halm, D., Grandidier, J.C. and Villalonga, S. (2014), "A fixed directions damage model for composite materials dedicated to hyperbaric type iv hydrogen storage vessel-part i: model formulation and identification", *Int. J. Hydrog. Energy*, **40**(38), 13165-13173.

Ramirez, J.P.B., Halm, D., Grandidier, J.C. and Villalonga, S. (2015b), "A fixed directions damage model for composite materials dedicated to hyperbaric type iv hydrogen storage vessel - part ii: validation on notched structures", *Int. J. Hydrog. Energy*, **40**(38), 13174-13182.

Ramirez, J.P.B., Halm, D., Grandidier, J.C., Villalonga, S. and Nony, F. (2015a), "Experimental study of the thermomechanical behavior of wound notched structures", *Int. J. Hydrog. Energy*, **40**(38), 13148-13159.

Rousseau, J., Perreux, D. and Verdière, N. (1999), "The influence of winding patterns on the damage behaviour of filament-wound pipes", *Compos. Sci. Technol.*, **59**(9), 1439-1449.

Sun, J. and Qi, X. (2006), "Elastic modulus prediction of filament winding composites based on meso-scale filament undulation property analysis", *Fuhe Cailiao Xuebao/acta Materiae Compositae Sinica*, **23**(6), 192-198.

Uddin, M.S., Morozov, E.V. and Shankar, K. (2014), "The effect of filament winding mosaic pattern on the stress state of filament wound composite flywheel disk", *Compos. Struct.*, **107**(1), 260-275.

Wen, W.D., Li, J., Cui, H.T., Xu, Y. and Zhang, H.J. (2011), "Strain characteristic of filament wound composite cylinder under axial loading", *Adv. Mater. Res.*, **415-417**, 395-398.

Zindel, D. and Bakis, C.E. (2011), "Nonlinear micromechanical model of filament-wound composites considering fiber undulation", *Mech. Compos. Mater.*, **47**(1), 73-94.

CC